Click Here for Full Article

Seismic structure of the Longmen Shan region from S-wave tomography and its relationship with the Wenchuan Ms 8.0 earthquake on 12 May 2008, southwestern China

Yi Xu,[1] Zhiwei Li,[1] Runqiu Huang,[2] and Ya Xu[1]

Received 19 November 2009; revised 22 December 2009; accepted 4 January 2010; published 30 January 2010.

[1] Using arrival time data, we determined seismic structure of the Longmen Shan by S-wave tomography and studied its relations with the Ms 8.0 earthquake in Wenchuan, southwestern China. Our results suggest that the Longmen Shan fault belt is a rheologic boundary between the eastern Tibetan plateau and the Sichuan basin, and the deep crust of the entire Longmen Shan is significantly thickened by ductile deformation. The upper structure of the eastern Tibetan plateau is cored by the high-velocity Pengguan massif. Its collision with the Sichuan basin is the most direct reason for the seismic ruptures on the Longmen Shan fault belt north of Wenchuan, while the lack of earthquakes south of Wenchuan is related to the weakness of the crust. Therefore, The Ms 8.0 earthquake occurred in a strongly heterogeneous region. The variations in the crustal structure largely controlled the initial rupture of the Ms 8.0 earthquake and aftershock activity. **Citation:** Xu, Y., Z. Li, R. Huang, and Y. Xu (2010), Seismic structure of the Longmen Shan region from S-wave tomography and its relationship with the Wenchuan Ms 8.0 earthquake on 12 May 2008, southwestern China, *Geophys. Res. Lett.*, *37*, L02304, doi:10.1029/2009GL041835.

1. Introduction

[2] On 12 May 2008, a great *Ms* 8.0 earthquake occurred in Wenchuan, southwestern China (Figure 1), with a focal depth of 16~18 km and a seismic rupture over 300 km along the Longmen Shan fault belt [*Huang et al.*, 2008; *Chen et al.*, 2009]. Located on the eastern margin of the Tibetan plateau, the Longmen Shan fault belt consists of three west-dipping thrust faults: the Wenchuan-Maoxian fault, the Yingxiu-Beichuan fault and the Guanxian-Jianyou fault, along which the mountain thrusts toward the foreland of the Sichuan basin. However, the Cenozoic slip rate of the Longmen Shan fault belt is only 2–3 mm/yr [*Burchfiel et al.*, 2008; *Zhang et al.*, 2008]. Together with GPS measurement data across the eastern margin of the Tibetan plateau [*Shen et al.*, 2005; *Gan et al.*, 2007], they suggest a slow convergence between the eastern Tibetan plateau and the Sichuan basin. As the eastward movement of the Tibetan plateau is obstructed by the strong lithosphere of the Sichuan basin, the crust of the Longmen Shan is significantly thickened [*Zhao et al.*, 2008; *Wang et al.*, 2008; *Lou et al.*, 2009; *Liu et al.*, 2009; *Wang et al.*, 2009] and the mountain is greatly elevated. Although the occurrence of the Wenchuan *Ms* 8.0 earthquake is attributed to thrusting of the Longmen Shan fault belt, some questions remain unclear. For example, what are the relations between seismic ruptures and crustal structures along the Longmen Shan fault belt? Why did the initial rupture of the main shock occur in Wenchuan but not the other parts of the Longmen Shan? Why did most of aftershocks occur on the northern Longmen Shan fault, while the region south of Wenchuan is almost aseismic? To answer these questions, we imaged the seismic structure of the Longmen Shan and its surrounding area by *S*-wave tomography to explore its relations with the occurrence of the *Ms* 8.0 earthquake.

2. Data and Method

[3] The data used in this study are *S*-wave arrival times of local/regional earthquakes recorded by the Sichuan Earthquake Network. Our study is focused on the Longmen Shan and surrounding areas. In order to sample deep crust by seismic rays at regional distances, we enlarge the data window to an area between 98°E~108°E and 25°N~35°N (Figure 2). The locations of these earthquakes are used as initial source parameters in the input data.

[4] Most of the selected earthquakes and recording stations are distributed in the eastern margin of the Tibetan plateau. The rest are sparsely distributed within the Sichuan basin. We extracted the earthquake data from January 2000 to April 2008, and those data after 12 May 2008 were excluded from our dataset. The first reason is that much of them are aftershocks of the *Ms* 8.0 earthquake, and they are overly concentrated on the Longmen Shan fault belt. The second reason is that the main shock created a ~300 km long rupture along the fault belt, and the earthquake data before the main shock were not affected by the change in the crust. In total, we selected ~58,000 *S*-wave arrival times from over 5800 earthquakes. Each earthquake was recorded by at least 5 stations. The residuals of the arrival times relative to an initial model were required to be less than ±3.0 sec. Final data show a good coverage in the study area, particularly in the Longmen Shan region (Figure 2).

[5] We determined the initial *S*-wave model based on the *P*-wave velocity model from a previous tomographic study in the eastern Tibetan plateau [*Xu*, 2004]. Firstly, the *S*-wave velocities at depths were obtained using a ratio of $Vp/Vs = 1.73$, and they were modified iteratively by calculating a set of synthetic travel times to fit actual arrival time data. Next, we refined the Moho of the study area using the gravity data described by *Jiang and Jin* [2005]. This is because there is a rapid increase in crustal thickness from the Sichuan basin to the eastern Tibetan plateau, whereas existing data from

[1]Key Laboratory of Petroleum Resource Research, Institute of Geology and Geophysics, Chinese Academy of Sciences, Beijing, China.
[2]State Key Laboratory of Geohazard Prevention and Geoenvironment Protection, Chengdu University of Technology, Chengdu, China.

Copyright 2010 by the American Geophysical Union.
0094-8276/10/2009GL041835$05.00

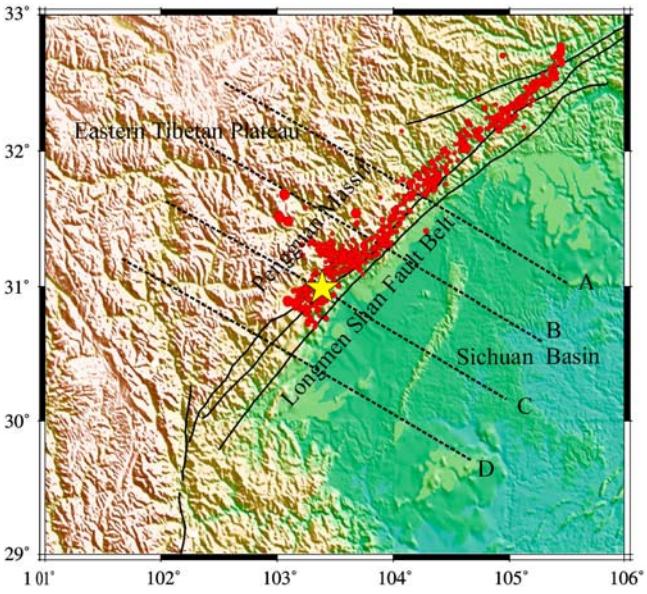

Figure 1. Tectonic outline of the Longmen Shan fault belt and locations of the *Ms* 8.0 earthquake (yellow star) and its aftershocks (red circles). The black solid lines are major faults; the dash lines are positions for four cross-sections.

seismic sounding profiles could not place good constraints on spatial variation of the Moho depth in the study area. We noted that the Moho depth calculated from the gravity data is comparable with those from seismological studies across the Longmen Shan fault belt [*Wang et al.*, 2008; *Lou et al.*, 2009; *Liu et al.*, 2009]. It was therefore used to calculate synthetic travel times in the ray tracing based on the initial model. Data coverage and resolution tests suggested that the study area could be divided by a set of grid spacings of 0.20° × 0.125° in longitudes and latitudes, by velocity discontinuities in the initial model at depths.

[6] The pseudo-bending ray tracing algorithm was used to calculate the *S*-wave travel times from the earthquake source to the recording stations in the initial model [*Zhao et al.*, 1992; *Koketsu and Sekine*, 1998], in which station elevation is taken into account. Earthquake locations and velocity parameters at grid nodes were inverted simultaneously and iteratively using a damped *LSQR* algorithm [*Paige and Saunders*, 1982]. The first iteration of the inversion was performed based on the 1-D layered velocity model, and its output result is a 3-D velocity model to include lateral variations corresponding to better-known shallow structures. It was used as the input model in next iteration. After several iterations, a small model variance indicates the final solution approached. Since data outliers and unevenness of ray paths tend to make the linear equation systems ill-conditioned, we also used smoothness constraints to control unreasonable local anomalies in inversion results [*Lees and Crosson*, 1989].

[7] A conventional checkerboard test was performed to examine resolution levels. The input model consisted of a set of alternating positive and negative velocity perturbations. Both of them had the maximum amplitude of ±0.4 km/s relative to the background velocity in the initial model. Real source-station pairs were selected to calculate synthetic travel times for the input model. The synthetic data were then inverted using the same tomographic procedures as that for the real data to recover the input model. The results of the checkerboard test show that input model can be resolved reasonably well (Figure 3). It is apparent that acceptable resolution can be achieved in the Longmen Shan and surrounding area using the existing earthquake data and seismic stations. The resolution is particularly good at depths of 10~20 km due to the better sampling of the crossing ray paths. At shallow depths, the Sichuan basin is not well resolved due to lack of ray paths. At depths of 30~40 km, acceptable resolution is obtained beneath the Longmen Shan. This is due to the better sampling of crossing ray paths at regional distances. In general, the results of the checkerboard test reveal a good degree of recovery in the Longmen Shan and surrounding area.

3. Result

[8] Our final results are shown Figure 4. *S*-wave velocity variations are described by perturbations relative to the background velocity in the initial model. Major fault lines, topography, locations of the relocated *Ms* 8.0 earthquake and aftershocks [*Chen et al.*, 2009] are plotted on these images.

[9] There is a good correlation between the velocity pattern and surface geology at the depths of 5~10 km. Bordered by the Longmen Shan fault belt, high velocities appear in the eastern Tibetan plateau which is cored by the Precambrian basement and highly metamorphosed rock in the Pengguan massif; low velocities appear in the foreland of the Sichuan basin where it is filled by thick Mesozoic and Cenozoic sediments. Most earthquakes are localized at the depth of 10 km, and they are mainly distributed on the boundary between the high and low velocities. At the depths of 15~20 km, high velocities tend to converge beneath the Longmen Shan fault belt. A lot of earthquakes occurred at this depth range, including the *Ms* 8.0 earthquake in Wenchuan. We note that region south of the Wenchuan is characterized by low velocities

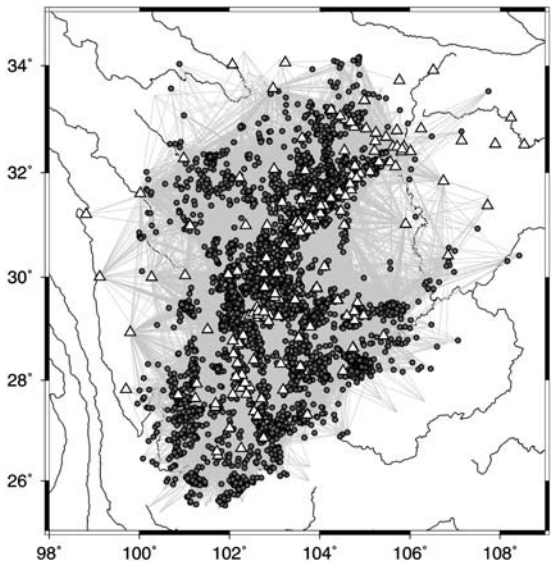

Figure 2. Locations of the seismic stations (white triangles) and earthquake sources (dark circles) in the study area. The gray lines are the *S*-wave ray paths of between the earthquake sources and the recording stations.

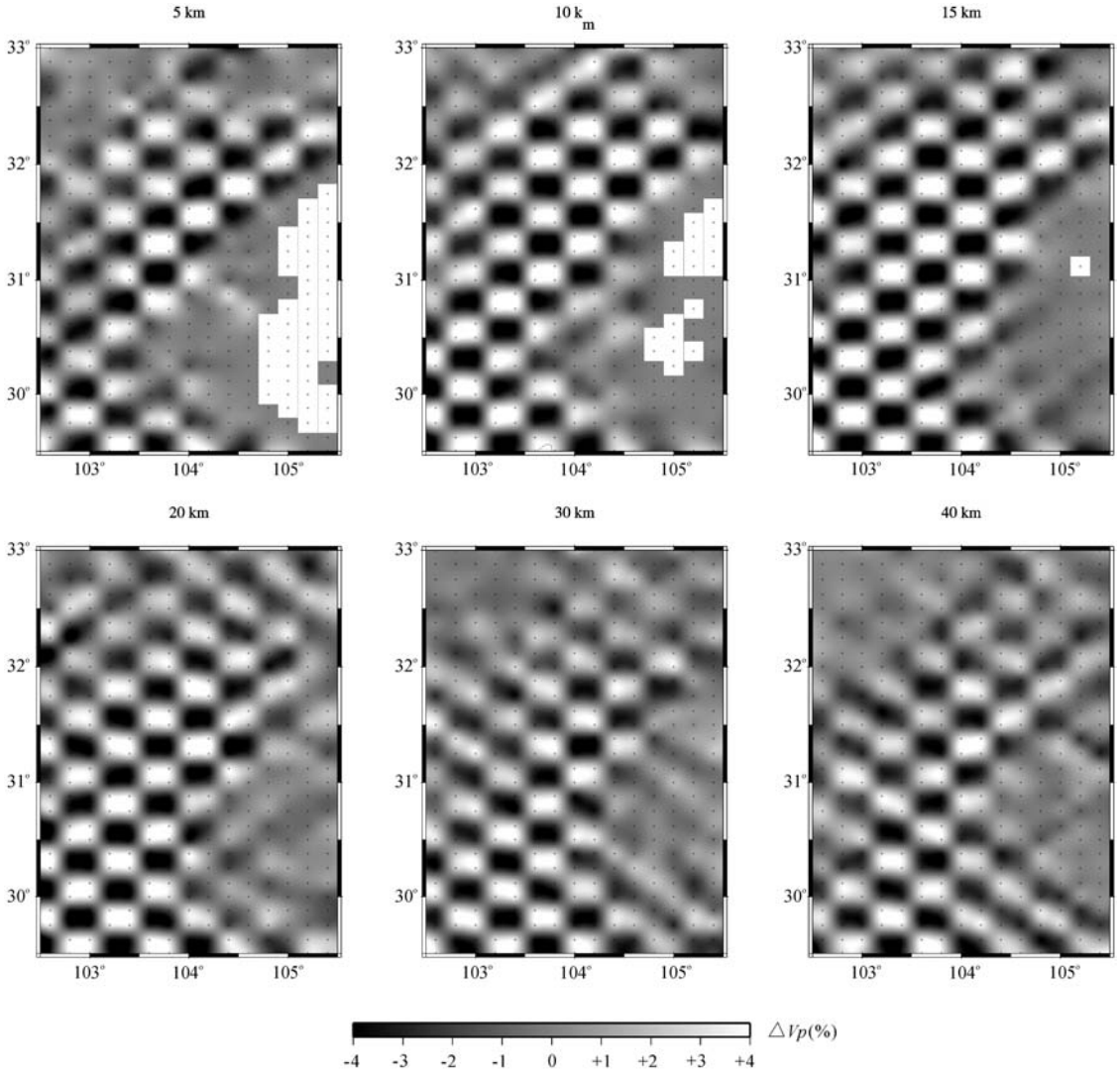

Figure 3. Recovered S-wave velocity checkerboard models. The input model consists of alternating positive and negative perturbations, with the maximum amplitudes of ±0.4 km/s over the reference velocity in the initial model.

where there are few earthquakes. The velocity pattern becomes reversed at the depth of 30 km. Low velocities appear in the eastern Tibetan plateau; high velocities appear in the Sichuan basin. Their boundary remains coincident with the downward projection of the Longmen Shan fault belt. This pattern seems continuous to the depth of 40 km, but there are almost no earthquakes at greater depths.

[10] Figure 5 are four *S*-wave velocity sections across the Longmen Shan fault belt. The most consistent feature is that the deep crust of the Longmen Shan has a thick low-velocity zone; the foreland of the Sichuan basin is filled with thick low-velocity sediments overlying the high-velocity crust. The Longmen Shan fault belt is imaged as a velocity transition boundary between them. The Moho depth increases from ~40 km beneath the Sichuan basin to ~60 km beneath the eastern Tibetan plateau, revealing a prominent thickening of the ductile crust. The main difference in the upper structure of the Longmen Shan is that on the sections A, B and C, the region north of Wenchuan has a high-velocity upper crust and most of the relocated earthquakes are concentrated at the depths of 10~20 km beneath the Longmen Shan; on the section D, however, the region south of Wenchuan has a low-velocity upper crust where no earthquakes occurred beneath the Longmen Shan.

4. Discussion

[11] The results from above analysis reveal a potentially spatial correlation between the Longmen Shan fault belt and the *S*-wave velocity structure, particularly on the eastern margin of the Pengguan massif. They reflect a rheologic difference of the crust across the fault belt. The high-velocity Pengguan massif is a main area that easily accumulates regional stress for seismic ruptures, but the deep crust of the entire Longmen Shan is thickened by ductile deformation and the Moho is flexed downward. In contrast, the foreland of the Sichuan basin is filled with thick sediments and underlain by a high-velocity crust. The Longmen Shan fault belt is localized on the narrow boundary between two reversed velocity structures. Moreover, the rheologic difference is

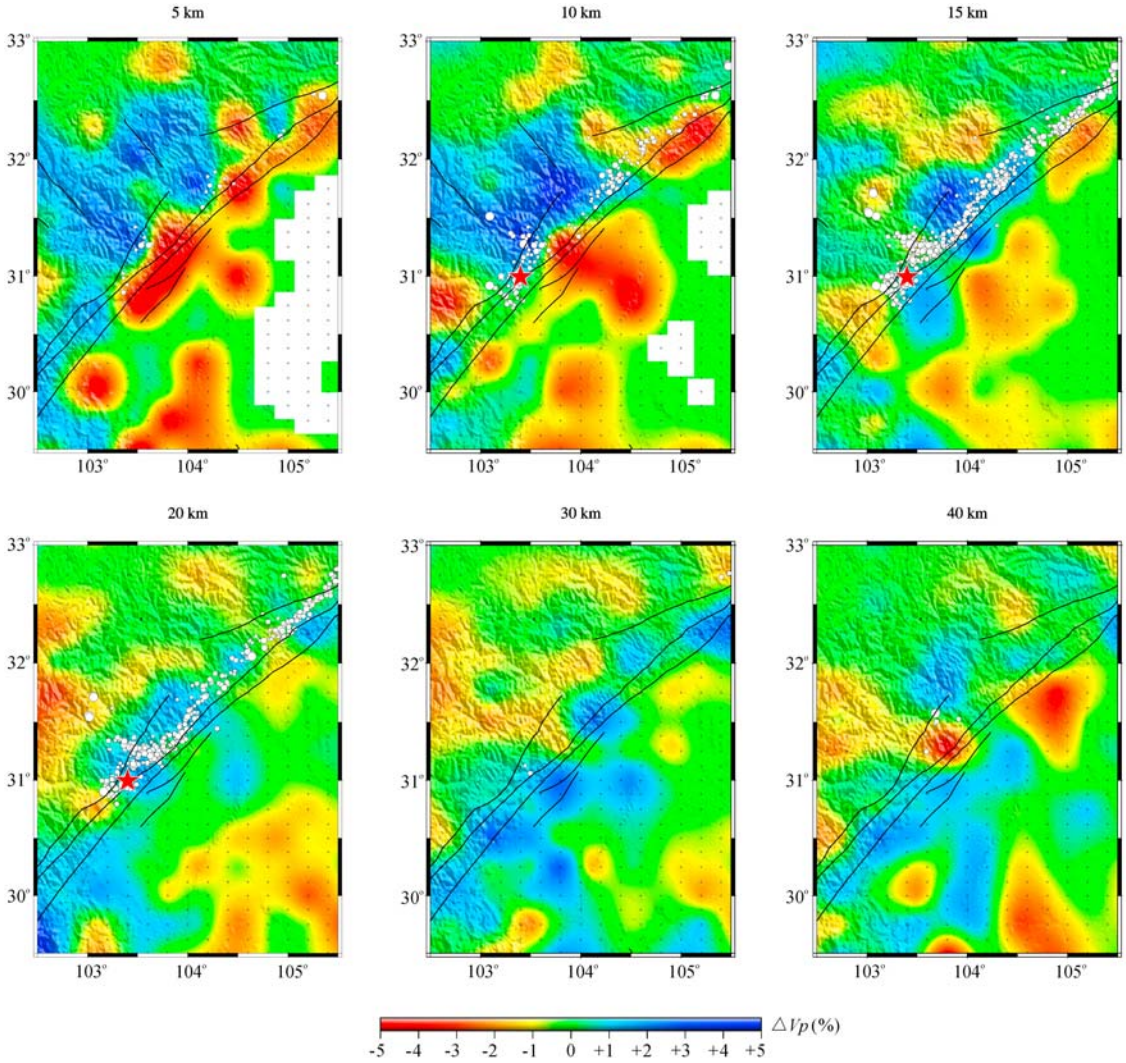

Figure 4. *S*-wave velocity variations in the Longmen Shan and surrounding area. They are shown in perturbations relative to the reference velocity in the initial model.

observed along the Longmen Shan fault belt. Compared to the Pengguan massif on the north, the crust south of Wenchuan is relatively weak. Such large rheologic variations in the crust have great effects on structural deformation on the Longmen Shan fault belt [*Clark and Royden*, 2000; *Cook and Royden*, 2008].

[12] Most earthquakes north of Wenchuan occurred on the eastern margin of the Pengguan massif. They are located between the base of the massif and the top of the high-velocity crust of the Sichuan basin. Clearly, due to the eastward movement of the Tibetan plateau, the stress accumulation in the Pengguan massif and its collision with the crust of the Sichuan basin are the most direct reasons to create seismic ruptures beneath the Longmen Shan. As for the lack of the seismic activity south of Wenchuan, it may be related to the weakness of the crust. Both historic and recent strong earthquakes occurred on the northern Longmen Shan fault belt but not in the region south of Wenchuan. Surface folding and faulting south of the Pengguan massif is distributed in a relatively wide region between the mountain and the basin [*Burchfiel et al.*, 2008]. Taken together, they suggest a decrease of the rheologic strength in the crust.

[13] The *Ms* 8.0 earthquake occurred in a highly heterogeneous area, which lead to an uneven regional stress accumulation around Wenchuan. Even if ductile deformation dominates the mid-lower crust of the Longmen Shan, the seismic ruptures are most likely to occur on the eastern margin of the Pengguan massif; comparably, seismic ruptures are not likely to occur in the region south of Wenchuan due to the weakness of the crust. Thus, the rheologic differences in the crustal structure have great effects on the earthquake activity north and south of Wenchuan. These tectonic conditions largely controlled the initial rupture of the *Ms* 8.0 earthquake and aftershock activity.

5. Conclusion

[14] We performed the *S*-wave tomography to analyze the seismic structure of the Longmen Shan and its relations with the *Ms* 8.0 earthquake in Wenchuan. Our result reveals two reversed velocity structures across the Longmen Shan fault belt. The high-velocity Pengguan massif is a main area for regional stress accumulation in the central Longmen Shan,

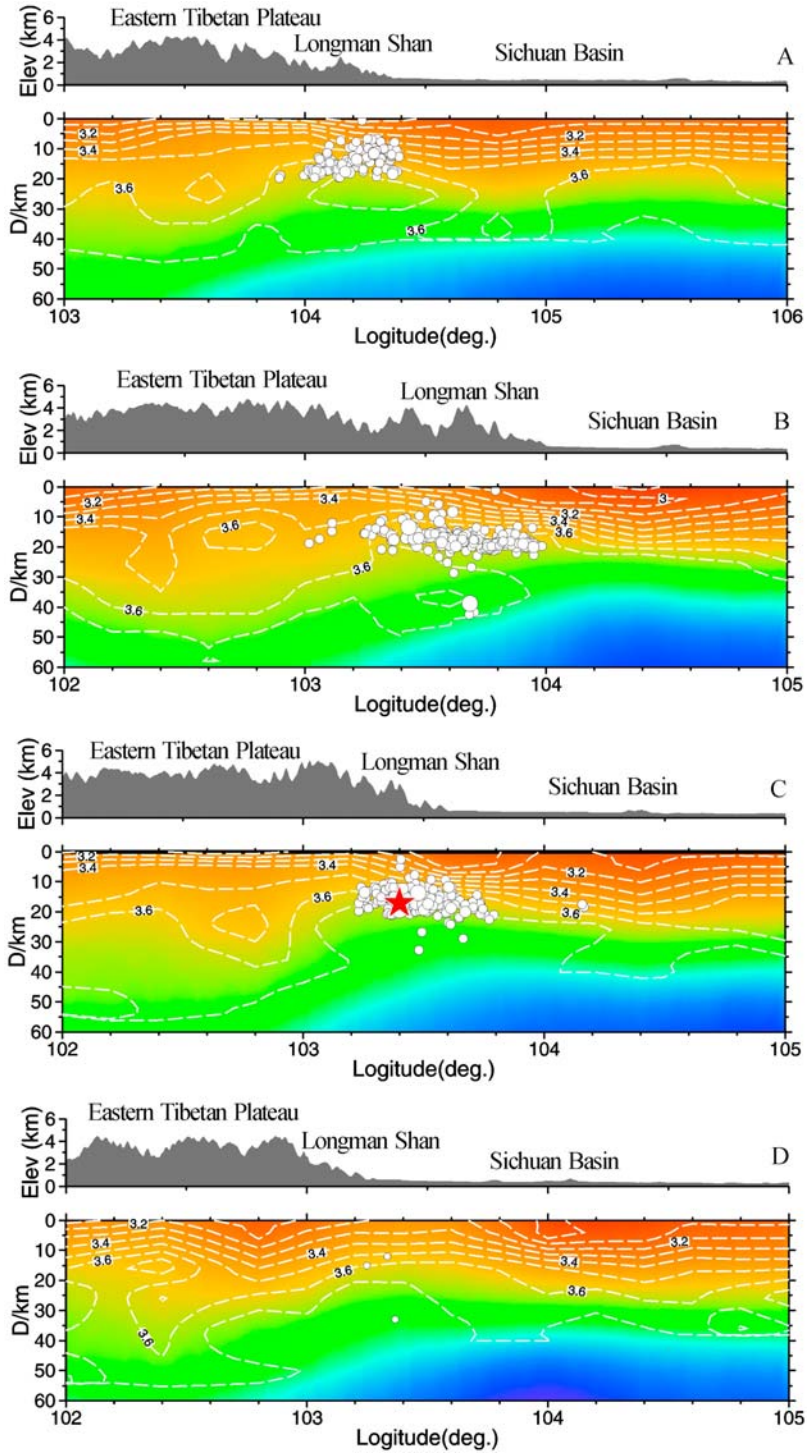

Figure 5. *S*-wave velocity sections across the Longmen Shan fault belt. Their locations are shown in Figure1. The white circles are the relocated earthquakes by *Chen et al.* [2009].

while the deep crust of the entire Longmen Shan is significantly thickened by the ductile deformation. The collision of the Pengguan massif with the crust of the Sichuan basin is the most direct reason for the seismic ruptures along the Longmen Shan fault belt north of Wenchuan; the lack of seismic activity in the region south of Wenchuan is related to the decrease of rheologic strength in the crust. The *Ms* 8.0 earthquake occurred in a strongly heterogeneous area around Wenchuan. The variations in the crustal structures largely controlled the initial rupture of the *Ms* 8.0 earthquake and aftershock activity.

[15] **Acknowledgments.** We thank the staff of the Sichuan Earthquake Network for providing valuable earthquake data. We also thank two reviewers for their valuable comments and suggestions. This study was supported by the State Key Laboratory of Geohazard Prevention &

Geoenvironment Protection, Chengdu University of Technology (grant DZKJ-0803), Chengdu, China.

References

Burchfiel, B. C., L. H. Royden, R. D. van der Hilst, B. H. Hager, Z. Chen, R. W. King, C. Li, J. Lü, H. Yao, and E. Kirby (2008), A geological and geophysical context for the Wenchuan earthquake of 12 May 2008, Sichuan, People's Republic of China, *GSA Today*, *18*(7), doi:10.1130/GSATG18A.1.

Chen, J. H., Q. Y. Liu, S. C. Li, B. Guo, Y. Li, J. Wang, and S. H. Qi (2009), Seismotectonic study by relocation of the Wenchuan Ms 8.0 earthquake sequence, *Chin. J. Geophys.*, *52*(2), 390–397.

Clark, M. K., and L. H. Royden (2000), Topographic ooze: Building the eastern margin of Tibet by lower crustal flow, *Geology*, *28*(8), 703–706, doi:10.1130/0091-7613(2000)28<703:TOBTEM>2.0.CO;2.

Cook, K. L., and L. H. Royden (2008), The role of crustal strength variations in shaping orogenic plateaus, with application to Tibet, *J. Geophys. Res.*, *113*, B08407, doi:10.1029/2007JB005457.

Gan, W., P. Zhang, Z. K. Shen, Z. Niu, M. Wang, Y. Wan, D. Zhou, and J. Cheng (2007), Present-day crustal motion within the Tibetan Plateau inferred from GPS measurements, *J. Geophys. Res.*, 112, B08416, doi:10.1029/2005JB004120.

Huang, Y., J. P. Wu, T. Z. Zhang, and D. N. Zhang (2008), Relocation of the *M*8.0 Wenchuan earthquake and its aftershock sequence, *Sci. China Ser. D Earth Sci.*, *51*(12), 1703–1711, doi:10.1007/s11430-008-0135-z.

Jiang, X., and Y. Jin (2005), Mapping the deep lithospheric structure beneath the eastern margin of the Tibetan Plateau from gravity anomalies, *J. Geophys. Res.*, *110*, B07407, doi:10.1029/2004JB003394.

Koketsu, K., and S. Sekine (1998), Pseudo-bending method for three-dimensional seismic ray tracing in a spherical earth with discontinuities, *Geophys. J. Int.*, *132*(2), 339–346, doi:10.1046/j.1365-246x.1998.00427.x.

Lees, J. M., and R. S. Crosson (1989), Tomographic inversion for three-dimensional velocity structure at Mount St. Helens using earthquake data, *J. Geophys. Res.*, *94*, 5716–5728, doi:10.1029/JB094iB05p05716.

Liu, Q. Y., Y. Li, J. H. Chen, B. Guo, S. C. Li, J. Wang, X. Q. Zhang, and S. H. Qi (2009), Wenchuan Ms 8.0 earthquake: Preliminary study of the S-wave velocity structure of the crust and upper mantle, *Chin. J. Geophys.*, *52*(2), 309–319.

Lou, H., C. Y. Wang, Z. Y. Lu, Z. X. Yao, S. G. Dai, and H. C. You (2009), Deep tectonic setting of the 2008 Wenchuan Ms8.0 earthquake in southwestern China-Joint analysis of teleseismic P-wave receiver functions and Bouguer gravity anomalies, *Sci. China Ser. D Earth Sci.*, *52*(2), 166–179, doi:10.1007/s11430-009-0009-z.

Paige, C. C., and M. A. Saunders (1982), LSQR: An algorithm for sparse linear equations and least squares problems, *Trans. Math. Software*, *8*(1), 43–71, doi:10.1145/355984.355989.

Shen, Z. K., J. Lu, M. Wang, and R. Burgmann (2005), Contemporary crustal deformation around the southeast borderland of the Tibetan Plateau, *J. Geophys. Res.*, *110*, B11409, doi:10.1029/2004JB003421.

Wang, C. Y., H. Lou, Z. Y. Lu, J. P. Wu, L. J. Chang, S. G. Dai, H. C. You, F. T. Tang, L. P. Zhu, and S. Paul (2008), S-wave crustal and upper mantle's velocity structure in the eastern Tibetan Plateau—Deep environment of lower crustal flow, *Sci. China Ser. D Earth Sci.*, *51*(2), 263–274, doi:10.1007/s11430-008-0008-5.

Wang, X. B., Y. T. Zhu, X. K. Zhao, N. Yu, K. Li, S. Q. Gao, and Q. L. Hu (2009), Magnetatelluric sounding new evidence to thrust belt structure in Longmen Shan, *Chin. J. Geophys.*, *52*(2), 564–571.

Xu, Y. (2004), Seismic tomography and deep tectonics of the Songpan-Aba region, research report, Explor. South. Co. of China Petrol. and Chem. Corp., Chengdu, China.

Zhang, P. Z., X. W. Xu, X. Z. Wen, and Y. K. Ran (2008), Slip rates and recurrence intervals of the Longmen Shan active fault zone and tectonic implications for the mechanism of the May 12 Wenchuan earthquake, 2008, Sichuan, China, *Chin. J. Geophys.*, *51*(4), 66–107.

Zhao, D., A. Hasegawa, and S. Horiuchi (1992), Tomographic imaging of P and S wave velocity structure beneath northeastern Japan, *J. Geophys. Res.*, *97*, 19,909–19,928, doi:10.1029/92JB00603.

Zhao, G. Z., X. B. Chen, L. F. Wang, J. J. Wang, J. Tang, Z. S. Wan, J. H. Zhang, Y. Zhan, and Q. B. Xiao (2008), Evidence of crustal "channel flow" in the eastern margin of Tibetan Plateau from MT measurements, *Chin. Sci. Bull.*, *53*(12), 1887–1893, doi:10.1007/s11434-008-0081-3.

R. Huang, State Key Laboratory of Geohazard Prevention and Geoenvironment Protection, Chengdu University of Technology, Chengdu 610059, China. (hrq@cdut.edu.cn)

Z. Li, Y. Xu, and Y. Xu, Key Laboratory of Petroleum Resource Research, Institute of Geology and Geophysics, Chinese Academy of Sciences, PO Box 9825, Beijing 100029, China. (zwli@mail.iggcas.ac.cn; xuya@mail.iggcas.ac.cn; xuyi@mail.iggcas.ac.cn)